FEATURE ARTICLE

ChemComm
www.rsc.org/chemcomm

Beyond crystallography: the study of disorder, nanocrystallinity and crystallographically challenged materials with pair distribution functions

Simon J. L. Billinge[a] and M. G. Kanatzidis[b]

[a] *Department of Physics and Astronomy and Center for Fundamental Materials Research, Michigan State University, East Lansing, MI 48824*

[b] *Department of Chemistry and Center for Fundamental Materials Research, Michigan State University, East Lansing, MI 48824*

Received (in Cambridge, UK) 11th August 2003, Accepted 17th November 2003
First published as an Advance Article on the web 2nd March 2004

Studying the structure of disordered and partially ordered materials is notoriously difficult. Recently, significant advances have been made using the atomic pair distribution function (PDF) analysis of powder diffraction data coupled with the use of advanced X-ray and neutron sources and fast computers. Here we summarize some of the more spectacular successes of this technique in studying the structure of complex materials and compounds. Our purpose is to make the PDF analysis technique familiar to the chemical community by describing its methodologies and highlighting its potential in solving structural characterization problems that are intractable by any other technique available to this community *e.g.* single crystal diffraction, Rietveld refinement of powder diffraction data and extended X-ray absorption fine structure analysis (EXAFS).

Introduction

The knowledge of structure is one of the key pillars of modern chemistry and the ability to determine it in almost all types of compounds (organic, inorganic, biological) has been the basis for the spectacular advances in nearly all physical sciences in the last nearly 100 years. The determination of structure in the vast majority of cases is due to the development of single crystal and powder X-ray crystallographic techniques. A prerequisite to a successful structure determination is the availability of high quality single crystals and, in the last two decades even polycrystalline powders. Nevertheless a number of compounds and materials have resisted this type of analysis because they are not fully periodic, are nanocrystalline, or are highly disordered. These are substances that do not crystallize (*e.g.* glasses and liquids) or crystallize to a limited degree (*e.g.* nanocrystals, gels, turbostratic materials, and various disordered systems). These systems are crystallographically intractable. In recent years a different approach has been developed that can tackle the structural issues in many of these systems to a high degree of accuracy. This approach centers around the atomic pair distribution function (PDF) technique.

The PDF analysis of powder diffraction data has been used for many years for studying materials with no long-range order such as glasses and liquids.[1] More recently with the advent of high power X-ray and neutron sources and fast computing, it is making an impact in the area of crystalline materials and as we will show here it has the potential to influence chemical science in a very positive way.[2,3] Traditionally, powerful crystallographic methods whereby Bragg-peaks are analyzed directly in reciprocal space provide extensive and sufficient information about the underlying structure. However, as interest shifts to more disordered crystals, and materials where the crystallinity itself is highly compromised (nanocrystals or "structurally challenged materials" as we define below), more and more critical information is contained in the *diffuse* scattering component. The PDF technique, and closely related total-scattering methods, allow both the Bragg and diffuse scattering to be analyzed together without bias, revealing the short and intermediate range order of the material regardless of the degree of disorder. This paper is intended to present an overview of some of the possibilities by referring to a number of recent examples where application of these techniques has revealed new information. For the reasons we outline here we anticipate the impact of the PDF technique to chemistry to be significant. Our aim is to introduce synthetic and structural chemists to the considerable possibilities offered by this method to solving structures that are otherwise intractable by standard and established crystallographic techniques.

Atomic pair distribution function technique

The PDF technique takes advantage of the Fourier relationship between measurable diffraction intensities and the real-space arrangement of pairs of atoms. The pair distribution function can be defined directly in real-space in terms of atomic coordinates. It can also be written as a Fourier transform of scattered X-ray or neutron intensities, as summarized below. In contrast to crystallographic methods, no presumption of periodicity is made allowing non-periodic structures, or aperiodic modifications to otherwise crystallographic materials, to be studied. It is also a highly intuitive function since peaks in the PDF come directly from pairs of atoms in the solid. For example, a peak that is shifted to lower-*r* therefore directly implies that this pair of atoms has a shorter bond. This

Simon J. L. Billinge is a Professor of Physics at Michigan State University where he joined in 1994 following a two-year Director's funded post-doctoral appointment at Los Alamos National Laboratory. His Ph.D was obtained in 1992 in Materials Science from University of Pennsylvania with a Bachelor of Arts from University of Oxford. His a research centers on applying novel X-ray and neutron scattering techniques to study the structure of complex materials, and using these methods to investigate important questions in physics and chemistry. Notable recent work was the first direct observation of the polaronic lattice distortion as charges localize at the metal–insulator transition in colossal magnetoresistant manganites, and the development of nanocrystallography described in this article. The work has resulted in more than 100 research publications and a recent book.

Mercouri G. Kanatzidis is a Distinguished Professor of Chemistry at Michigan State University where he has served since 1987. Prior to that he was a postdoctoral research associate at the University of Michigan and Northwestern University from 1985 to 1987. He received his Ph.D. degree in chemistry from the University of Iowa in 1984, after getting a Bachelor of Science degree from Aristotle University in Greece. His research has generated seminal work in metal chalcogenide chemistry through the development of novel "solvents" for solid state synthesis including flux methods, hydrothermal and solvothermal techniques. He is currently working on new thermoelectric materials, the synthetic design of framework solids, intermetallic phases and nanocomposite materials. The bulk of his work is described in the more than 400 research publications.

DOI: 10.1039/b309577k

directly measurable function therefore provides a very nice quantitative template against which one can test one's chemical intuition. Below we briefly define the functions and mention how they can be measured. Much more detail is available in a recent book on the subject, "Underneath the Bragg Peaks: Structural Analysis of Complex Materials".[2]

The experiments are straightforward X-ray and neutron powder diffraction measurements. They are typically carried out at synchrotron X-ray sources and pulsed neutron sources, rather than on laboratory sources, because it is important to measure data over a wide range of momentum transfer, Q, for high accuracy and adequate real-space resolution of the PDF peaks. Since Q is given by, $Q = 4\pi\sin\theta/\lambda$ (for elastic scattering), and Q's of > 30 Å^{-1} are desirable, this implies that short-wavelength, high energy, X-rays or neutrons are required. X-rays of > 45 keV ($\lambda = 0.27$ Å) and up to 100 keV ($\lambda = 0.12$ Å) or more are typically used. Data from laboratory sources with Mo or Ag tubes can give acceptable results, but working at a synchrotron or spallation neutron source is always to be preferred for the highest resolution measurements. In the future beamlines that are optimized for this kind of measurement will make these synchrotron experiments very straightforward. Information about developments in this regard, and contacts of people for collaborations, can be found on the web-page: www.totalscattering.org.

The atomic PDF, $G(r)$, is defined as

$$G(r) = 4\pi r[\rho(r) - \rho_o], \tag{1}$$

where ρ_o is the average atomic number density, $\rho(r)$ is the atomic pair-density defined below and r is a radial distance.[1] The function $G(r)$ gives information about the number of atoms in a spherical shell of unit thickness at a distance r from a reference atom. It peaks at characteristic distances separating pairs of atoms. An example of $G(r)$ from fcc nickel is shown in Fig. 1(b).

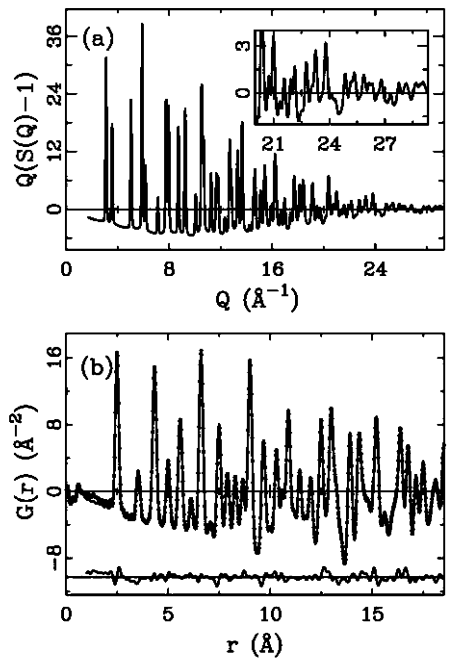

Fig. 1 (a) The reduced structure function, Q[S(Q)-1], of crystalline Ni. Data were collected at RT at beamline ID-1 of the Advanced Photon Source at Argonne National Laboratory. (b) The PDF obtained by Fourier transforming the data in (a).

As mentioned, $G(r)$ is an experimentally accessible function. It is related to the measured X-ray or neutron powder diffraction pattern through a Fourier transform; in detail,

$$G(r) = (2/\pi)\int_{Q=o}^{Q_{max}} Q[S(Q)-1]\sin(Qr)dQ, \tag{2}$$

where $S(Q)$, the total scattering structure function, contains the measured intensity from an isotropic sample such as a powder and is defined below. An example of $S(Q)$ from nickel, measured over a wide range of Q at beamline ID-1 of the Advanced Photon Source in Argonne National Laboratory and plotted as the reduced structure function, $Q[S(Q) - 1]$, is shown in Fig. 1(a). The structure function is related to the coherent part of the total diffracted intensity of the material,

$$S(Q) = \frac{I^{coh}(Q) - \sum c_i |f_i(Q)|^2}{\left|\sum c_i f_i(Q)\right|^2} + 1 \tag{3}$$

where $I^{coh.}(Q)$ is the measured scattering intensity from a powder sample that has been properly corrected for background and other experimental effects and normalized by the flux and number of atoms in the sample. Here, c_i and f_i are the atomic concentration and X-ray atomic form factor, respectively, for the atomic species of type i.[1,2] In the case of neutron experiments the f's are replaced by Q-independent neutron scattering lengths, b, and the sums run over all isotopes and spin-states as well as over the atomic species. The choice between carrying out a neutron or X-ray experiment depends on the nature of the sample and what information is sought. As we show below, the old paradigm that neutrons were intrinsically superior to X-rays for this kind of measurement, because there is no neutron atomic form factor killing intensity at high-Q, is no longer valid with the advent of extremely intense high energy X-ray synchrotron beams that can accurately measure scattered intensity at very high Q values.

As can be seen from eqns. (1)–(3), $G(r)$ is simply another representation of the diffraction data. However, exploring the diffraction data in real space has advantages especially in the case of materials with significant structural disorder, as we discuss below. The PDF reflects both the long-range atomic structure, manifest in the sharp Bragg peaks, and the local structural imperfections, manifest in the diffuse components of the diffraction pattern. This is because (eqns. (2) and (3)) the *total* scattering, including Bragg peaks as well as diffuse scattering, contributes to the PDF. The analysis of the data also does not presume periodicity. Therefore, this technique is particularly useful for characterizing aperiodic distortions in crystals.

The data are corrected for experimental effects such as sample absorption, multiple scattering, and so on, and normalized to get the structure function $S(Q)$. This process is described in detail elsewhere[2,4,5,6] and various programs are available for carrying out these corrections.[7,8,9,10] Imperfect corrections result in distortions to $S(Q)$ but these distortions vary much more slowly than the signal and are manifest as sharp peaks at very low-r in the PDF in a region (< 1.0 Å) where no structural information exists.[2] The PDF is rather robust against data processing errors, though having said that one should be warned against over interpreting individual features in the PDF, especially at lower-r values. A significant advantage of the PDF is that the useful structural data persist to very long r distances allowing models to be fit over significant ranges. Providing they are not over-parameterized, these fits are highly resistant to random and systematic errors in the data and provide robust structural solutions†.

Modeling the PDF is straightforward because it can be calculated directly from a structural model using

$$G(r) + 4\pi r\rho_0 = \frac{1}{r}\sum_{\nu}\sum_{\mu}\frac{f(0)_\nu f(0)_\mu}{\langle f(0)\rangle^2}\delta(r - r_{\nu\mu}) \tag{4}$$

† As with any structure refined from powder diffraction data, the structural solutions are not unique, but they are robust in the same sense that Rietveld refined structures are and yield meaningful quantitative structural parameters.

Here the *f(0)*'s are the atomic form factors evaluated at $Q = 0$ that are, to a good approximation, given by the number of electrons on the atom, *Z*. In the case of neutron diffraction the *f(0)*'s should be replaced by neutron scattering lengths, b_ν. In eqn. 4, $r_{\nu\mu}$ is the distance separating the νth and μth atoms and the sums are over all the atoms in the sample.[2] For a material whose structure can be described by a small unit cell, which in general for the case of disordered crystals will be a supercell of the crystallographic cell, the first sum in (4) runs over atoms in the cell and the second sum runs over all atoms up to whatever cutoff, r_{max}, may be of interest. This makes the problem computationally significantly more tractable! A number of regression programs are available. A program that uses least-squares in analogy with Rietveld refinement is PDFFIT.[11] Alternative approaches include using a reverse Monte-Carlo type approach where a residuals function is minimized using a simulated annealing algorithm[12] or using some kind of potential based modeling scheme.[13,14,15] These approaches have been summarized and compared elsewhere.[2]

Below we illustrate some of the recent advances in the manner and scope of the application of PDF methods to disordered-crystalline and nanocrystalline materials. This is intended as an introduction to the chemistry community of some of the possibilities of the technique and is not a comprehensive review. It draws heavily on our own work at Michigan State University and it is not intended as an exhaustive account of work done in this area.

High-resolution X-ray PDF measurements

The technological development that motivated the recent developments in PDF's applied to crystalline materials was the advent of spallation neutron sources. Unlike reactor sources, these have high fluxes of epithermal neutrons with short wavelengths. The real-space resolution of the PDF is directly related to the range of *Q* over which data are measured; roughly speaking $\delta r = \pi/Q_{\max}$ where Q_{max} is the maximum *Q*-value. Since $Q = 4\pi\sin\theta/\lambda \leq 4\pi/\lambda$, to increase Q_{max} it is necessary to decrease λ. Spallation neutron sources, for the first time, provided an abundance of neutrons of short enough wavelength to make studies of crystalline materials, with their sharp and closely spaced PDF peaks, of interest. These pulsed neutron PDF studies on crystalline materials have had some notable successes since 1987 when they were first carried out.[16,17,18,19,20]

Increasing the real-space resolution of *X-ray* measurements presents an additional challenge: the X-ray form-factor, *f(Q)*. The square of this is a measure of the structural-information containing coherent scattering from the material under study. The structure factor falls off sharply with increasing *Q* resulting in a weak signal at high diffracting angles. This is illustrated in Fig. 2(a) that shows the raw intensity from WS_2 (described below). The overall drop-off in intensity follows $|f(Q)|^2$ with very little apparent structure in the scattering in the high-*Q* region. However, when the data are divided by $|f(Q)|^2$, as per eqn. (2), diffuse structure becomes apparent in this region (Fig. 2(b)). It is therefore important to measure to these high-*Q* values with good statistics. This does not present a problem when new high-flux, high-energy synchrotrons are used such as Cornell High Energy Synchrotron Source (CHESS) and the Advanced Photon Source (APS) at Argonne National Laboratory. The incident flux at high energies is so great that, despite the inefficient coherent scattering, sufficient statistics can be obtained to yield accurate data up to at least 45 $Å^{-1}$.

Solid solutions and the collapse of Vegard's law

The potential of this technique was shown in the case of the solid solution series of semiconductors, $In_{1-x}Ga_xAs$.[6,21] The high quality data from the $In_{1-x}Ga_xAs$ series, measured at CHESS at 10 K, are shown in Fig. 3(a) with the high-*Q* region magnified. Noise is apparent, but the signal, a sine-wave feature with a period ~0.2Å, is clearly evident especially in the alloys where Bragg-peaks at high-*Q* are suppressed by the alloy-induced structural disorder. When these data are Fourier transformed they result in the PDF's in Fig. 3(b). What is clearly apparent is that the nearest neighbor In–As peak is split into two, partially resolved, peaks in the alloys. The short Ga–As and long In–As bonds survive almost unstrained in the alloy. Extensive modeling of the data, including comparison with chemically specific but low spatial resolution differential PDF's obtained using anomalous diffraction methods,[22] resulted in a fairly complete understanding of the local structure of these technologically important alloys and confirmed, but significantly expanded, the information available from earlier XAFS studies.[23] Normally, these systems obey the so-called Vegard's Law, which implies that all metric parameters from the unit cells to the bond lengths vary smoothly with *x*. The PDF analysis shows that Vegard's Law can be misleading when considering the local structure of solid solutions.

PDF for glasses: what is old is new again

These technique developments, motivated by the desire to study crystals, have now been fed back into the traditional study of glasses. Of interest here is the ability to study covalently bonded network glasses such as silicates and aluminosilicates. In this case the structural coherence is limited to less than 10 Å due to the random orientations of connected tetrahedra, and peaks in the PDF beyond first and second neighbors are broad. However, PDF peaks originating from the SiO_4 tetrahedra themselves are extremely sharp because of the well-defined covalent bonding and rigidity of the unit. The ability to resolve the short and long bonds in the semiconductor alloys that differed by only 0.14 Å motivated a study of aluminosilicate glasses.[24] These materials consist of continuous covalently bonded random networks of corner shared tetrahedra; however, some of the tetrahedra contain silicon and others aluminium. There are diverse types of aluminosilicates, many with very interesting and useful properties. In fact zeolites, widely used for catalysis and molecular encapsulation, are crystallographically

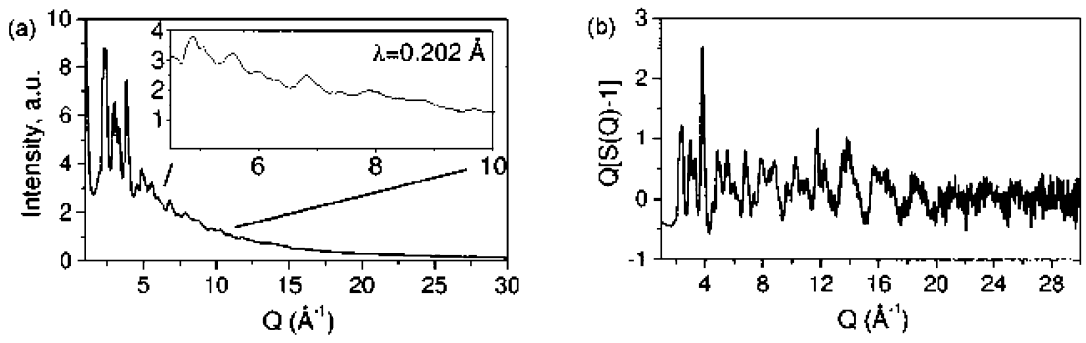

Fig. 2 (a) Raw intensity data from a sample of exfoliated-restacked WS_2 measured using X-rays of $\lambda = 0.202$ Å ($E \sim 60$ keV) from CHESS. This Figure illustrates the effect of the atomic form-factor in suppressing intensity at high-*Q*. (b) The same data after making corrections and dividing by $|f(Q)|^2$ showing significant diffuse intensity in the high-*Q* region.

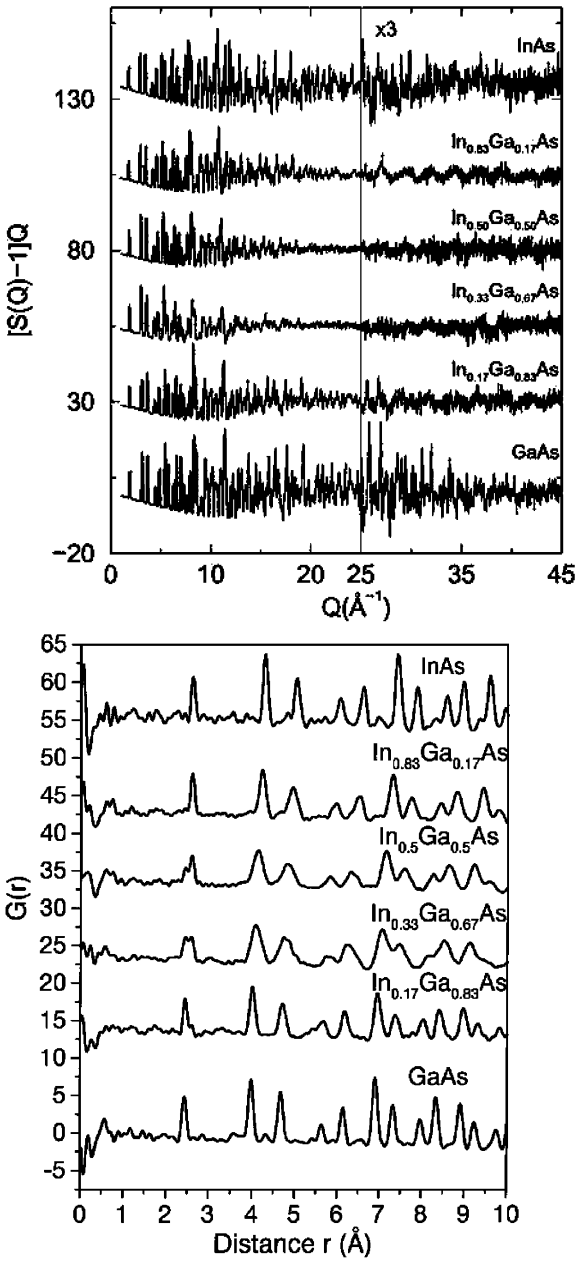

Fig. 3 (a) The reduced total scattering structure functions *[S(Q)−1]Q* for $In_xGa_{1-x}As$ measured at 10K. The data-sets from the different members of the alloy series are offset for clarity. The high-*Q* region is shown on an expanded scale (×3) to highlight the presence of the diffuse scattering. (b) The PDFs, *G(r)*, obtained from the data in (a) by Fourier transformation. Note the nearest neighbor peak is split into two components in the alloys.

ordered aluminosilicate networks. Despite their importance these materials present special challenges in their structural characterization. In general, the Al and Si ions are arrayed randomly. They are close in the periodic table making it hard to differentiate them by scattering power in an X-ray experiment, and by quirk of fate, they have similar neutron scattering lengths too. They are low atomic number materials making XAFS measurements difficult, and NMR signals get broad when the Al and Si coexist. However, when they form their tetrahedra with oxygen the Si–O bond is shorter than the Al–O bond by around 0.14 Å. In a high real-space resolution PDF measurement it was possible to *spatially* resolve the Si–O and Al–O peaks and watch how the peak intensities, widths and positions shifted with changes in the composition.[24] The *Q*-space structure functions and the PDF's are shown in Fig. 4. In Fig. 5 the *G(r)* functions are shown on an expanded *r*-scale with fits to the Si–O and Al–O sub-components of the peaks. The data were collected at ID1 of the Advanced Photon Source. This is a particularly nice example where chemical specific analysis is a special challenge because of randomly arranged low-*Z* (and similar) constituents, but where the chemistry of the different species could be studied independently by *spatially resolving* them due to the high real-space resolution attained.

Nanocrystals and crystallographically challenged materials

Crystals have long-range order. Their structure can be defined by a small number of parameters that define the unit cell (its shape and size) and its contents (atomic coordinates and thermal factors). The complete structure is then obtained by periodically repeating this unit cell *ad-infinitum*. Towards the opposite end of the structural order–disorder spectrum are glasses and liquids that have only short-range order and no long-range order. The local environment of a particular atom type may be well ordered, but the correlations die out over the range of a few angstroms, as discussed above in relation to Fig. 4(b). In this case, the complete structure is never completely "solved", but is described statistically in terms of atomic distributions or atom-pair distributions.

Increasingly, new materials are being discovered that lie between these two extremes. They have a well-defined structure over local *and intermediate range* that can be described rather well by a small unit cell and a small number of parameters. However, they are not long-range ordered and the structural coherence dies out on a nanometer length-scale. We call these materials "nanocrystals". In these materials the scattering pattern either does not contain Bragg-peaks or contains very few making it impossible to study using conventional crystallographic techniques. We have demonstrated that the PDF is a tractable and intuitive approach to solving the structures of these materials resulting in robust and quantitative structural solutions.

Note that this definition of nanocrystals goes beyond perfect crystals that are simply very small (nanometer in size) such as passivated gold and semiconductor nanoclusters[25,26] and includes materials where the particle size can be larger but the *structural coherence* is at the nanometer length-scale. As we discuss below, this includes a large number of interesting materials. The important point is that the materials are ordered over a sufficiently long range to allow a concise description of the structure in terms of a small number of parameters, but are not ordered over sufficiently long range to allow a structural solution using conventional crystallographic techniques. Examples we have studied using the PDF technique include MoS_2 and related compounds[27,28] and $V_2O_5{\cdot}nH_2O$ xerogel.[29]

Another class of interesting materials are those where long-range order exists but where significant structural distortions are also present that are not reflected in the average structure. These can be considered as defects to the average structure, for example, in the case of the semiconductor alloys described above. However, sometimes the distortions are rather extensive, or it is the aperiodic component of the structure that is of particular interest, in which case it makes less sense to consider the disorder as a defect away from the ideal structure. This class of materials is rather widespread and includes extended solid sate compounds and even molecular systems, for example, plastic crystals that have periodically arranged but orientationally disordered molecules.

All of these materials, where deviations from perfect crystallinity are rather severe but a remnant of the crystallinity is apparent, we term "crystallographically challenged materials" to distinguish them, on the one hand, from well-ordered crystals and, on the other, glasses.

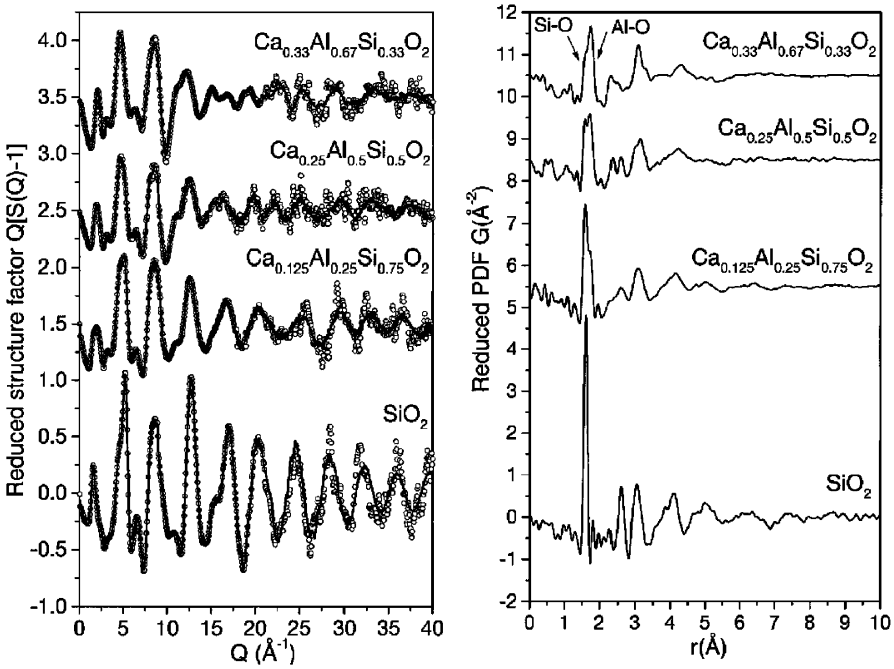

Fig. 4 (a) Structure functions from aluminosilicate glasses measured at the Advanced Photon Source to high-*Q* values. (b) Resulting PDFs, *G(r)*. Note that the characteristic glassy structure, with features disappearing by 10 Å, indicating the presence of only short-range order in the structure. However, what is also apparent is that the local structure is well defined, especially in the pure silica glass (bottom curve) with very sharp PDF peaks.

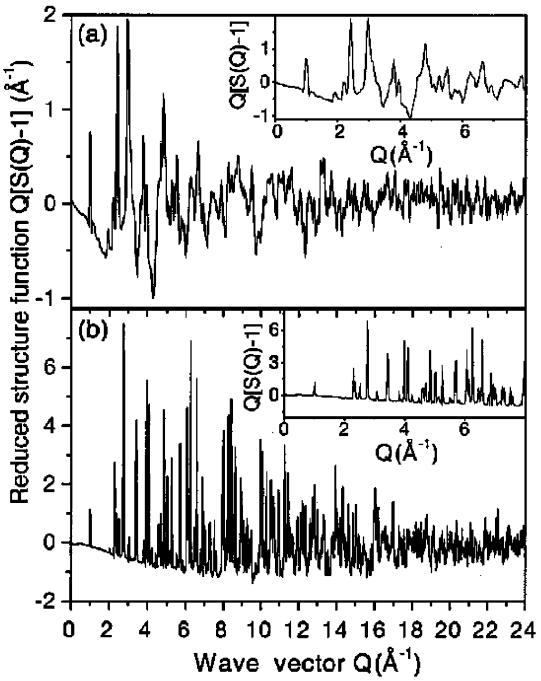

Fig. 5 Experimental structure functions of (a) $LiMoS_2$ and (b) MoS_2. Note the different intensity scale between (a) and (b). The data are shown in an expanded scale in the insets. Peaks in the nanocrystalline $LiMoS_2$ data are much broader.

Crystalline and nanocrystalline MoS_2 and its derivatives

As an example of nanocrystals we consider first the MoS_2 system. Pristine MoS_2 is the key catalyst for the removal of sulfur from crude oil (hydrodesulfurization).[30] The material is perfectly crystalline and consists of covalently bonded layers of Mo–S_6 trigonal prisms held together by Van der Waals forces. $LiMoS_2$ has Li intercalated between the MoS_2 layers. It is important as a precursor in the preparation of a variety of lamellar nanocomposites.[31] Despite being extensively studied for the last three decades the structure of $LiMoS_2$ could not be determined. The reason is that, on Li intercalation, pristine MoS_2 is dramatically modified resulting in a product that is too poorly diffracting to allow a crystallographic structural solution. This leaves unanswered the important question of what exactly happens to the Mo–S network when MoS_2 gets reduced with lithium.

X-Ray powder diffraction data from the MoS_2 and $LiMoS_2$ samples were measured at beamline X7A at NSLS. The reduced structure functions are shown in Fig. 5 and the resulting PDFs in Fig. 6. Sharp Bragg peaks are present in the *S(Q)* of MoS_2 up to the maximal *Q* value of 24 Å^{-1} (Fig. 6(b), the inset shows the data on an expanded scale. The scale was chosen to mimic what would have been measured on a laboratory X-ray source using Cu K_α radiation and measuring to very high diffraction angle). The corresponding

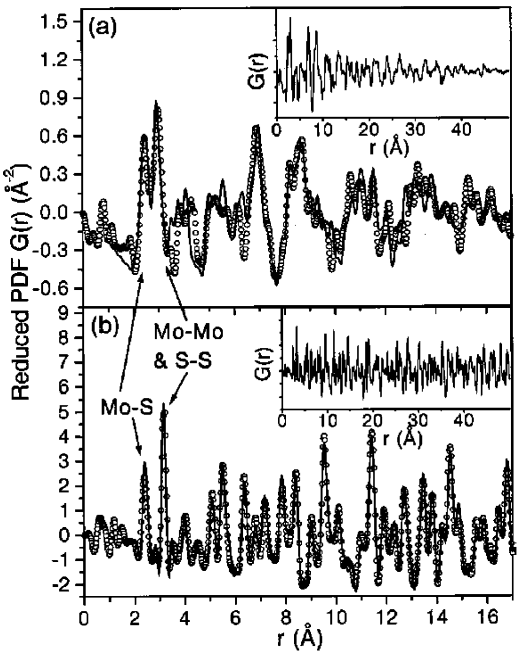

Fig. 6 PDFs from (a) $LiMoS_2$ and (b) MoS_2 from the data in Fig. 5 (dots). The experimental data are shown on an extended scale in the insets. Solid lines in the main panel are PDFs calculated from structural models.

G(r) also features sharp peaks reflecting the presence of well-defined coordination spheres in this "perfectly" crystalline material (Fig. 6(b)). The inset to Fig. 6(b) shows *G(r)* calculated to 5 nm. Clearly the amplitude of the structural features (the PDF peak:peak amplitude) remains unattenuated over this range as is expected for a long-range ordered material. This is a result of the sharp Bragg-peaks in *S(Q)* evident in Fig. 6(b). The known crystal structure also fit well to the PDF (solid line in the Figure). These results can be taken as unequivocal proof that pristine MoS_2 is not a "crystallographically challenged material" and that the reported crystal structure is in fact the correct one.

The data from the nanocrystalline $LiMoS_2$ sample serve to illustrate the problem of structure solution from this class of materials. Plenty of structure is evident in the scattering (Fig. 5(a)) but the peaks are broad and quickly become strongly overlapped. This is especially evident in the inset that can be compared with the data from crystalline MoS_2 in the inset to Fig. 5(b), plotted over the same range. Conventional crystallographic methods (*e.g.*, Rietveld) lose their power with data like this, which explains why a full 3-dimensional solution of the structure eluded scientists for so long. The Fourier transformed data (Fig. 6(a)) contain peaks of comparable sharpness to those from the crystalline material (the comparison is even more dramatic in the case of WS_2 described below and shown in Fig. 8) indicating that the local structure is well defined. On the other hand, features in *G(r)* die out with increasing *r* as shown in the inset to Fig. 7(a) that can be compared to the inset

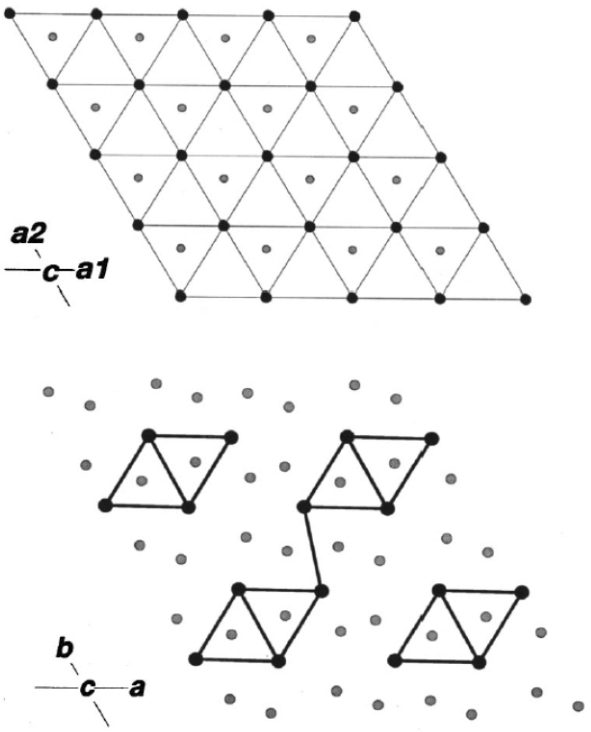

Fig. 7 Projection down the *c* axis of the crystal structures of hexagonal MoS_2 (upper) and triclinic $LiMoS_2$ (lower). The large black circles are Mo atoms and the small gray circles are the S atoms. Li atoms are not shown for the sake of clarity. In the $LiMoS_2$ structure the 6 second-neighbor Mo–Mo separations split into 3-long and 3-short.[29]

to Fig. 6(b) from the crystalline material. Oscillations in *G(r)* have virtually disappeared by 50 Å. The range of the structural coherence is therefore limited to ~5 nm, which results in the broad peaks in the diffraction pattern and justifies the characterization of "nano-crystalline".

The relatively sharp features in *G(r)* allow structural models to be compared to the data and differentiated. A number of structural models were fit to the $LiMoS_2$ data; the best fit of the most successful is also shown as a solid line in Fig. 7(a). Competing models produced qualitatively poorer fits.[29] The best-fit structural model showed the following. The Mo–S_2 layers in $LiMoS_2$ are built of distorted Mo–S_6 octahedra. In pristine MoS_2, the Mo atoms from a single Mo–S_2 layer arrange in a regular hexagonal lattice (see Fig. 7) and are all separated by the same distance of 3.16 Å. On the contrary, molybdenum atoms occupy two distinct positions in the triclinic unit cell of $LiMoS_2$ giving rise to short (2.9–3.10 A) and long (3.44–4.07 Å) Mo–Mo distances. As a result, triangulated diamond chains of short Mo–Mo distances are evident, as shown in Fig. 7.

The observed distorted structure of $LiMoS_2$ also has a strong physicochemical basis that can be understood in terms of simple electron counting arguments. In MoS_2 the molybdenum is in the 4+ state and has 2 *d*-electrons. It is stable in a prismatic crystal field resulting in a 1–3–1 arrangement of atomic *d*-energy levels. The two electrons both occupy the lowest energy level and are therefore paired. The Mo therefore has non-bonding interactions with its neighboring Mo ions resulting in 6 equal Mo–Mo distances. When Mo gets reduced by the addition of Li it has 3 *d*-electrons. The prismatic coordination is destabilized with respect to octahedral coordination that results in triply degenerate t_{2g} and doubly degenerate e_g orbitals. One electron goes into each of the 3 t_{2g} orbitals that point towards neighboring Mo ions. Each Mo can then form metal-metal bonding interactions with 3 of its neighboring Mo ions resulting in 3 shorter (and 3 longer) Mo–Mo bonds and the diamond like pattern of distortions shown in Fig. 7(b).

This also explains the zig-zag distortion pattern observed in exfoliated-restacked WS_2.[28] This material is isostructural and chemically very similar to MoS_2. Lithium can be intercalated to produce $LiWS_2$. The material can then be exfoliated in solution whereby the (Mo/W)S_2 layers separate and form a colloid. By changing the chemical conditions the layers can be restacked and the Li washed out. The resulting material is WS_2, chemically nearly identical to the starting material, but significantly modified structurally by the exfoliation-restacking process. The resulting structure is nanocrystalline and metastable, returning to the ground-state structure of pristine (Mo/W)S_2 over a period of hours in the case of MoS_2 and weeks for WS_2. The full 3-D structure of nanocrystalline WS_2 was solved for the first time by the PDF technique. The structure functions and PDFs of pristine and exfoliated-restacked WS_2 are shown in Figs. 8(a) and (b), respectively. In Fig. 8(b) the low-*r* peaks in the PDF of the nanocrystalline metastable phase are sharp and resolution limited testifying to the well defined order. However, the extent of the structural order is rather short-range, being already significantly attenuated by 20 Å in this case. The W–W peak at 3 Å in the pristine material splits into 4 peaks (2.77 Å, 2.85 Å, 3.27 Å and 3.85 Å) due to a zig-zag arrangement of short (~2.8 Å) and long (~3.5 Å) bonds.

In the case of exfoliated-restacked (Mo/W)S_2 the Mo/W is reduced by intercalating Li during the exfoliation process. It therefore transforms into the octahedral coordination similar to reduced $LiMoS_2$. When the Li is removed during restacking the W gets kinetically trapped in its octahedral environment. However, now there are only 2 electrons instead of 3 in the t_{2g} states. The W can only bond with two of its W neighbors instead of 3 and the distortion pattern is a one-dimensional zig-zag instead of the triangulated diamonds of $LiMoS_2$.

To summarize, in both Li intercalated and the exfoliated-restacked structures the material forms well-defined 3-dimensionally ordered structures that can be described with a rather small unit cell. However, structural coherence is limited to 5 nm or less, apparent as the fall-off in intensity in *G(r)* with increasing *r* (Figs. 6(a) and 8(b)). In *S(Q)* this is apparent as a profound broadening of the "Bragg-peak" intensity compared to those of the crystalline samples. Note, that despite the broad peaks in *S(Q)* for the nanocrystalline sample, sharp (resolution limited) peaks are evident in *G(r)*, confirming that the structure is locally very well defined

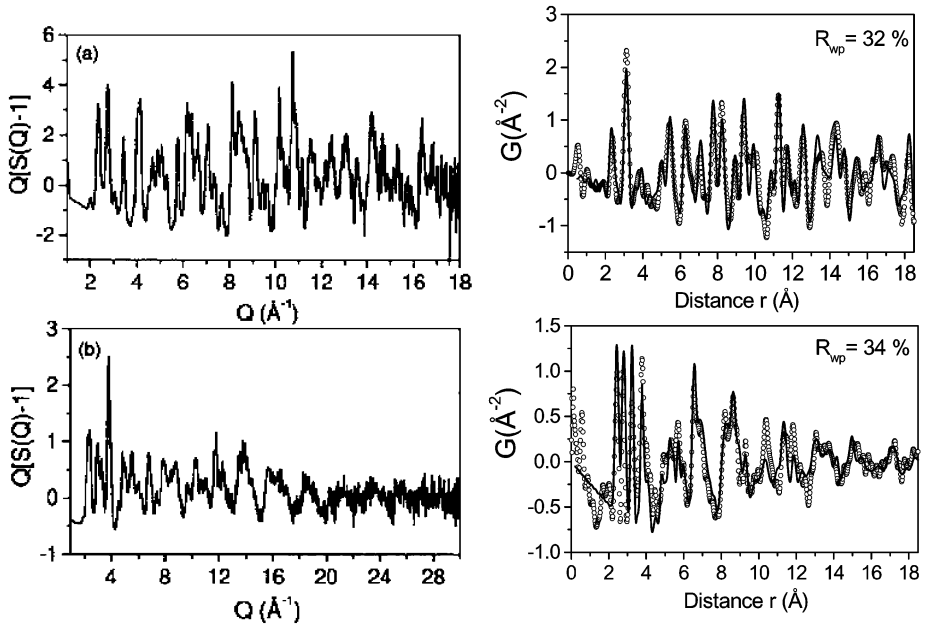

Fig. 8 Reduced structure functions (left), and PDFs (right), of (a) hexagonal pristine WS_2 and (b) exfoliated-restacked WS_2.

though the coherence of the order falls off with increasing-*r*. This is canonical "nanocrystalline" behavior.

Crystallographically challenged oxides of molybdenum

As well as the nanocrystalline sulphides of molybdenum described above, oxides of Mo with Mo in the reduced state also present interesting examples of crystallographically challenged materials that benefit from analysis using total scattering methods. Here we describe three examples from the work of Hibble and Hannon: namely $LiMoO_2$[32] Li_2MoO_3[33] and $LaMo_2O_5$.[34,35]

The case of $LiMoO_2$ is directly analogous to the $LiMoS_2$ described above, although in this case the material is not nanocrystalline: it diffracts with clear Bragg-peaks. The structure was solved using crystallographic methods and published.[36] It remained a "solved structure" for almost 10 years before the PDF of the material was checked. This immediately showed that the published structure was wholly inadequate, as shown in Fig. 9 (top panel). An alternative model was proposed that fit both the PDF data *and* the powder diffraction profile. Interestingly the original rhombohedral model of Aleandri and McCarley[38] had Mo sitting in a high symmetry position with six second neighbor Mo atoms at equal distances of 2.865 Å. The new model, which accounts also for the PDF data, has short and long Mo–Mo bonds indicating the existence of metal-metal bonding as expected in analogy with the $LiMoS_2$ example above. There are presumably more "solved" structures in the literature that would benefit from this kind of analysis!

Another similar example is that of Li_2MoO_3 whose structure was solved first by James and Goodenough[37] whose structural solution proved less than adequate when compared to PDF data. Again, short and long Mo–Mo bonds were missed in the original structural model that became immediately apparent when compared to the neutron PDF data. This is a particularly nice example where multiple techniques were used to get to the bottom of the problem, there being an XAFS study that indicated the presence of short and long Mo–Mo bonds and the full structural solution then being made on neutron powder data that were fit using both conventional Rietveld refinement and PDF methods.

The last example is particularly interesting since the structural solution that took into account the PDF data also indicated what had gone wrong with the original structural solution. In the case of $LaMo_2O_5$ the single crystal structure was always known to be

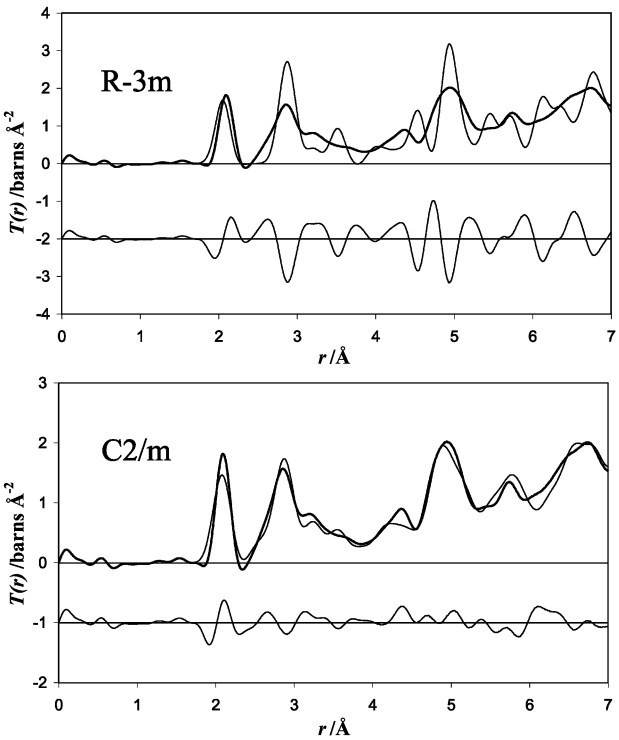

Fig. 9 Neutron PDF (in the form of the radial distribution function, *R(r)* (designated *T(r)* in the figure) of $LiMoO_2$ (thick line) compared with two models: (top panel) published crystallographic model (Aleandri and McCarley, 1988) and model determined using both Rietveld refinement and PDF data as inputs.

problematic since it yielded a solution containing atoms that approached each other too closely.[36,37] The single crystal structure, in space group $P6_3/mmc$, also gave poor agreement with the PDF. Two more physical structures were found that agreed rather well with the PDF. These were somewhat distorted from the single crystal structure and were described in lower symmetry sub-groups of the parent structure ($P\bar{3}m$ and $P6_3mc$). Furthermore, the two models had very similar short-range order up to around 10 Å. This suggested that perhaps both variants are actually present in the material intergrown into each other. The material is therefore

twinned on a nanometer length scale over which the crystallographic measurements (including powder diffraction in this case) average resulting in a crystallographically correct, but physically meaningless, structural solution. Again, comparing models with PDF data was central in sorting out this complicated situation. The resulting solutions also resulted in interesting and somewhat unexpected (though reasonable) structural motifs of Mo–O clusters and an interestingly triangulated Mo–Mo bonded network.

$V_2O_5{\cdot}nH_2O$ xerogel

Another important example is $V_2O_5{\cdot}nH_2O$ xerogel. This material has fascinated researchers in the decades since its discovery because of its exotic open nanoporous structure with many potential applications in science and technology.[38] Despite decades of extensive experiments with $V_2O_5{\cdot}nH_2O$ its 3-D atomic structure has not been determined in detail. The reason is that the xerogel exists only as ribbon-like particles about 10 nm wide and 1 μm long. Being such a poorly crystalline solid the xerogel exhibits a diffraction pattern without any Bragg peaks making it impossible to determine the 3-D atomic structure by traditional crystallographic techniques. Instead the diffraction pattern consists of a rather small number of quite sharp features, indicating intermediate range order, and a pronounced diffuse component, as we have discussed, characteristic of nanocrystalline materials. Again, the PDF method showed that this material is in fact nanocrystalline and allowed straightforward testing and refinement of 3-d structural models allowing a solution of the structure.

The structure functions for crystalline V_2O_5 and the $V_2O_5{\cdot}nH_2O$ xerogel are shown in Fig. 10 and the resulting PDFs are shown in

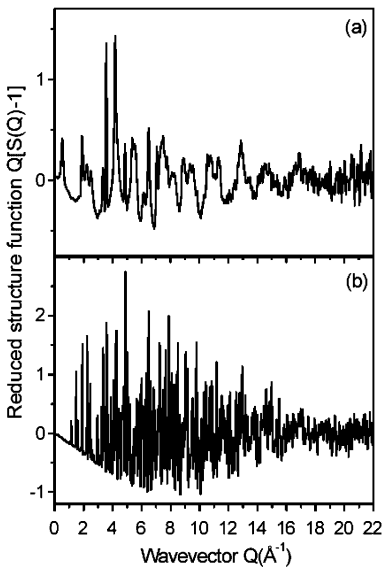

Fig. 10 Reduced structure functions, Q[S(Q) − 1], of (a) $V_2O_5{\cdot}nH_2O$ xerogel and (b) crystalline V_2O_5, collected at beamline X7A, NSLS.

Fig. 11.[30] The diffraction patterns are characteristic for crystals and nanocrystals with extensive Bragg peaks in the one case and well defined but relatively broad features in the other. Features are also evident at low-*Q* in the xerogel coming from the lamellar character of the structure. Again characteristic are the PDFs, *G(r)*. The crystalline material has sharp, well-defined PDF-peaks that extend indefinitely in-*r* (actually the range of *r* where features are seen in the PDF are determined by the *Q*-space resolution of the measurement). The peaks in the nanocrystalline xerogel are also sharp, especially below 12 Å (about which more later), but the peaks are gradually attenuated with increasing *r* as highlighted in the insets to Fig. 11.

Modeling the nanocrystalline *G(r)* revealed the following. In contrast to crystalline V_2O_5, which is an ordered assembly of single layers of VO_5 units, the gel is a stack of bi-layers of similar VO_5

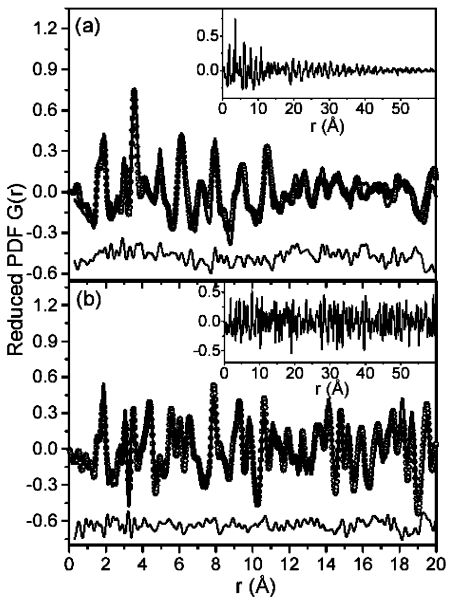

Fig. 11 Experimental (circles) and fitted (solid line) PDFs for (a) $V_2O_5{\cdot}nH_2O$ xerogel and (b) crystalline V_2O_5. The residual difference is shown in the lower part. The experimental data are shown over longer range in the insets to emphasize the nanocrystalline nature of the xerogel (inset in (a)).

pyramidal units with water molecules residing between the bi-layers with the distance of closest approach between the bi-layers being 11.5 Å. In addition to the regular VO_5 a sixth oxygen atom occupies what would be the sixth coordination site opposite to that of the doubly-bonded V=O oxygen but at a much longer distance of ~ 2.5 Å.

Sharp decreases in the structural coherence (the amplitude of features in the PDF) are apparent at around 11.5 Å and 23 Å (*e.g.*, see Fig. 11(a)). Such a slight but persistent loss of structural coherence repeatedly occurring at distances close to the (bi-layer)–(bi-layer) separation suggests that bi-layers in $V_2O_5{\cdot}nH_2O$ are not stacked in perfect registry indicating the presence of inter-bilayer stacking disorder. Poorly stacked layers can be mimicked in the PDF by artificially enlarging the atomic thermal factors in the out-of-plane direction, an approach that proved quite successful in modeling the turbostratic disorder in pyrolytic graphite.[31] The modified model yielded the PDF shown in Fig. 11(a). The observation of turbostratic disorder in these xerogels is in contrast to the considerable layer-layer correlation occurring in "restacked" WS_2 and $LiMoS_2$ discussed above. However, it is similar, and probably has a similar origin, to that observed in the pyrolitic graphite that we describe below. In that case it is believed to be coming largely from curvature of the graphene sheets. In the case of these xerogels the relatively long, narrow ribbons are known from TEM measurements to be highly curved and tangled which is possible if the bilayers remain in contact but are allowed to slide incoherently over one another.

Nanoclusters and atoms intercalated in materials

Nanoporous materials are important for their ability to store and sieve individual molecules.[39] Their large surface area also makes them important as hosts for catalysts. For example, one of the most important catalysts in petroleum cracking is nanoporous zeolite. There is also fundamental scientific interest in the behavior of materials under confinement. The practice of producing materials with atomic scale holes or pores, and filling them with things, will be around for some time to come. Obviously, it is important to be able to study the material intercalated in the pores or between the layers. Specifically, we would like to know the structure of materials intercalated into nanopores. The PDF can be very useful in this regard because periodicity of the structure is not a

prerequisite and so the intercalates need not be long-range ordered, which in general they are not. By using a differential technique such as anomalous X-ray scattering,[40] neutron isotope-exchange, or simply subtracting the scattered intensity from an empty host sample (i.e., considering the host to be the "sample container" and carrying out corrections accordingly), it is possible to extract the local structure in the vicinity of an intercalated atom or molecule. Because of signal-to-noise problems, this process is relatively in its infancy. However, a number of studies show that the approach is feasible. The structure of Se and CsSe and RbSe clusters intercalated in zeolites Y was solved using anomalous X-ray diffraction.[41] Also, the position and orientation of $CHCl_3$ in the supercages of NaY zeolites was determined by a hydrogen-deuterium isotope substitution experiment coupled with neutron PDF analysis.[42] By subtracting the scattering from an empty zeolite host it was also possible to study Cs intercalated into the zeolite ITQ-4.[43]

Based on spectroscopic measurements Cs intercalated into ITQ-4 was thought to be the first room-temperature stable electride material, but no direct structural evidence was available to support this. Electrides are interesting low-dimensional correlated electron materials. Ionic solids such as CsCl have a lattice of Cs^+ ions with Cl^- as counter-ions. Cs^+ can also be stabilized in solution when solvated by polarizable molecules. Electrides are at the interface of these extremes, where an ionic lattice forms from solvated alkali cations such as Cs^+ and the counter-ions are simply the donated electrons. In electrides the donated-electron density appears to be confined within cavities and channels in the matrix.[44] It behaves like a low-density correlated electron gas where the dimensionality of the electron gas and its electronic and magnetic properties are determined by the topology of the cavities in the host matrix. X-ray PDF measurements showed that, indeed, the intercalated Cs was in the Cs^+ state verifying that this is indeed an electride material. Furthermore, the Cs^+ ions arrange in zig-zag chains in the pores of the zeolites host (Fig. 12). The pores in the ITQ-4 are narrower than most zeolites (7 Å) and have an undulating 1-d topology as shown in Fig. 12(a). The scattering from the zeolites with and without loading is shown in Fig. 13(a) (note the Bragg-peaks with considerable diffuse scattering also present) and the resulting PDFs in Fig 13(b). Significant new peaks are evident in the PDFs of the Cs loaded zeolites around 4 Å. This is even more apparent in the Cs

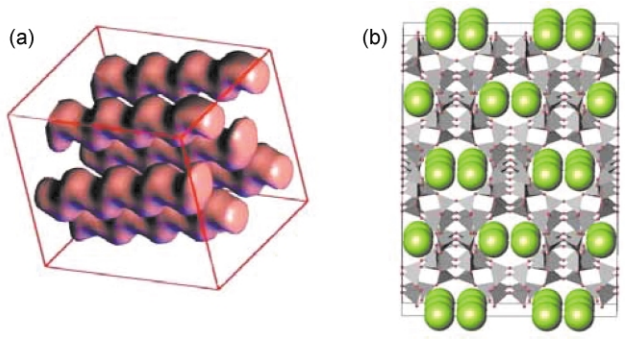

Fig. 12 (left) Representation of the pore topology in the zeolite ITQ-4. (right) Structural model of the Cs^+ ions intercalated in the pores of the zeolite host as determined using differential PDF methods.

differential PDFs shown in Fig 14. Both the total and differential PDFs were fit with models to arrive at the proposed structure of zig-zag chains of Cs atoms in the pores.

Another example of solving the structure of an intercalation compound is Ag_xMoS_2.[45] This material was prepared by encapsulating Ag+ ions with single layers of MoS_2. The product is highly disordered, possibly turbostratic and cannot be dealt with the Rietveld technique. The PDF analysis technique was employed to obtain full three-dimensional structure of this material. It was found that, at the atomic scale, this compound can be well described as an assembly of anionic MoS_2 slabs encapsulating the Ag^+ ions. Ag atoms are found in an almost linear coordination of two sulfur atoms at 2.41 and 2.46 Å. The molybdenum atoms engage in strong metal–metal bonding giving rise to Mo–Mo zigzag chains within the MoS_2 slabs just like restacked WS_2 discussed above. The new structural information obtained for Ag_xMoS_2 could not have been obtained by any other currently available technique.

PDF as a check of single crystal structure solutions

A number of the examples described above suggest that structures exist in the literature where the structure solution itself is "challenged", if not completely wrong. The PDF can be a useful check of these structure solutions since it is simply the atomic probability distribution of the material measured directly. The PDF from the proposed structural model can be straightforwardly

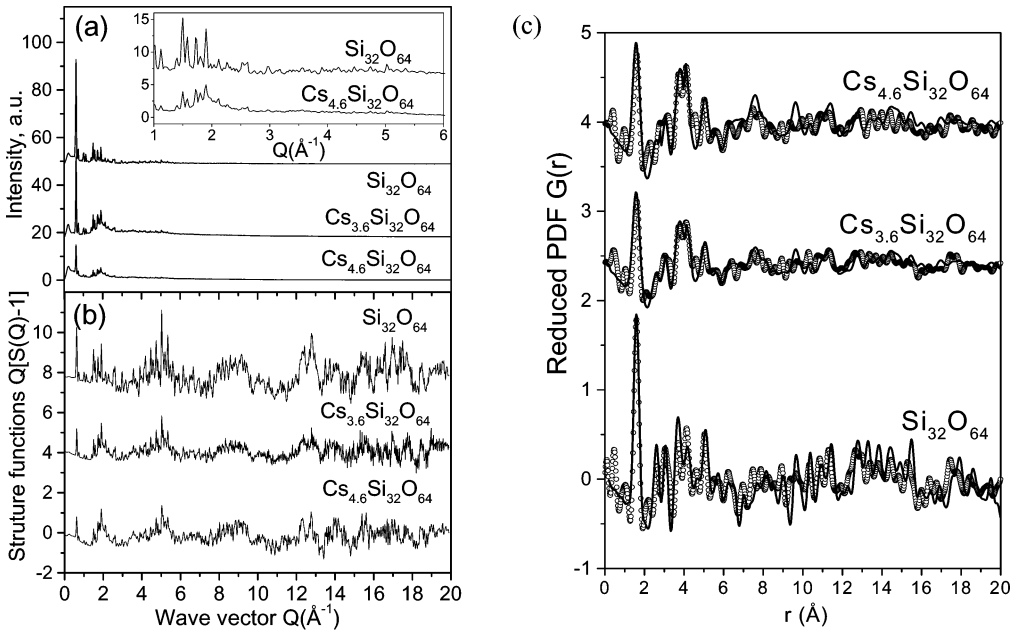

Fig. 13 (a) Raw X-ray powder diffraction data from bare ITQ-4 silica zeolites (top curves in each panel) and Cs loaded electride materials with two different Cs loadings (lower curves). Data were collected at room temperature using beamline X7A at NSLS. (b) Same data converted to the reduced structure function ready for Fourier transformation. Note the reproducible structural features at high-*Q* that are not immediately evident in the raw data. (c) PDFs from the data in (a) and (b). Dots are the measured data and solid lines are from the structural models. Note the strong increase in intensity of the feature around 4 Å.

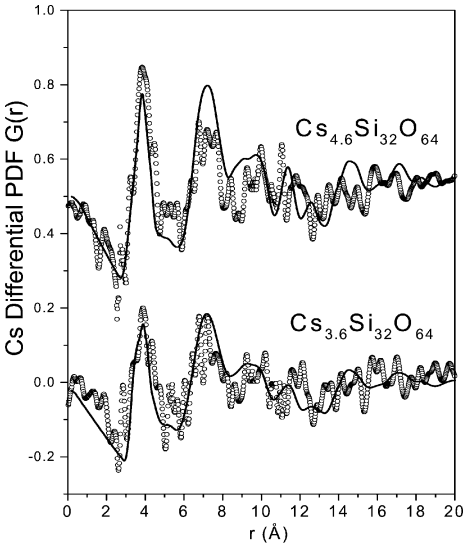

Fig. 14 Differential PDFs obtained by subtracting the scattering from the zeolite host (dots). Solid lines are calculated PDFs from models fit to both the differential and total PDFs. The models are the same except for taking into account the Cs loading. The only successful models involved Cs^+ indicating that the intercalated Cs is ionized in this material.

calculated (using PDFFIT for example) and compared to the data. For example, in the case of pristine MoS_2 this approach verified that the published crystal structure was indeed correct. In other cases, such as the Mo_2O_4, it identified problems with the published structural model. Another nice example where this was found to be the case is that of Cu_xUTe_3. The single crystal crystallographic analysis of Cu_xUTe_3 suggests the presence of straight chains of Te atoms (~ 3.0 Å apart) along the *a*-axis. This is an artifact, as shown by electron diffraction studies that indicate the existence of a supercell along the *a*-axis. Pair distribution function analysis (PDF) was used to show that the Te–Te chains contain Te–Te dimers at 2.74 Å.[46] This is the result of local distortions that can be discussed with respect to the parent binary phase, α–UTe_3. From the PDF it was found that, contrary to expectation, the two nearly isostructural phases, Cu_xUTe_3 and α-UTe_3, have substantially different local structures.

The PDF data obtained for α-UTe_3 and $Cu_{0.33}UTe_3$ are shown in Fig. 15. The peaks at low interatomic distance-*r* give us unique

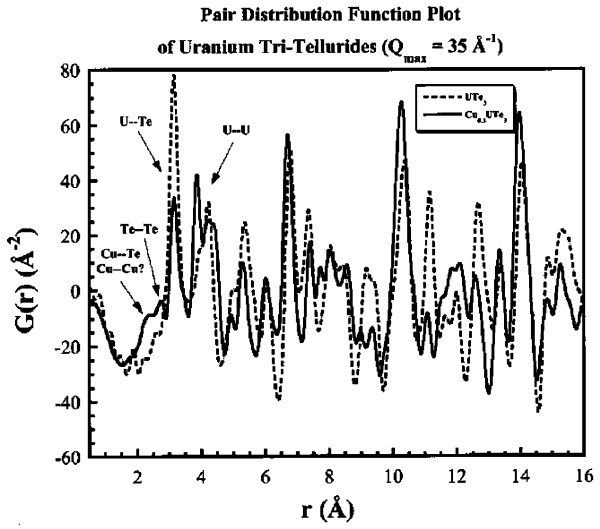

Fig. 15 PDF data obtained for α-UTe_3 and $Cu_{0.33}UTe_3$.

insight of the situation present in the first coordination sphere in both phases. In the copper intercalated phase, the peak at 2.75 Å is indicative of shortened Te–Te bonds, not present in the single crystal model. This argues strongly for significant local distortions, which may in fact be periodic as implied by the presence of the *a*-axis superstructure observed by electron diffraction. The weak, broad shoulder at ~ 2.5 Å is due to Cu–Te and possibly Cu–Cu vectors. The observation of *both* a clear 2.5 Å shoulder *and* a 2.75 Å peak is strong evidence for the presence of Cu in the intercalated material.

The large peaks at 3.15 Å in both phases correspond to the first U–Te coordination shell. The width of these peaks reflects the wide distribution of U–Te vectors present. At slightly longer distances in the PDF of $Cu_{0.33}UTe_3$ we observe peaks around 3.9 Å and 4.2 Å which correspond to Te–Te and U–U vectors. In the parent α-UTe_3, the single crystal model also indicates a single U–U distance of 4.22 Å, but the PDF of $Cu_{0.33}UTe_3$ clearly shows that the distribution of the 3.9 Å and 4.2 Å vectors is different, indicating a significant local distortion in the structure upon Cu insertion.

It is clear that the PDF data demonstrate the intercalation of copper into the α-UTe_3 structure, and the resulting compound has a distinct local structure, whilst at the larger distance regime, the overall structure appears qualitatively similar to the parent.

Another case in which the single crystal structure determination failed to capture the true picture is $K_2Th_2Se_6$.[47] In this case, the average single crystal structure suggested Se–Se contacts of 2.727 Å that lie right in the middle of the range of a single normal Se–Se bond at 2.34 Å and a van der Waals contact at 3.4 Å. If this were accurate, the Se–Se distance of 2.727 Å would be a truly novel feature of the structure and an example of rare, even unprecedented, Se–Se bonding worthy of extensive theoretical studies. Because of some apparent inconsistencies between spectroscopic data and the structural model we suspected the local structure associated with the Se–Se unit to be more complicated than depicted from the X-ray crystallographic results. Only PDF analysis indicated the presence of a Se–Se bond in the structure of 2.34 Å demonstrating that a local non-periodic distortion existed and showing that the observed distance of 2.727 Å was an artifact of averaging.

Rapid acquisition PDF: RAPDF

Data collection for PDFs involves relatively straightforward powder diffraction measurements. The main difficulties come from having to use high-energy X-rays and having a stable and low-background setup allowing reliable quantitative measurement of weak diffuse intensities. This is described in detail in Egami and Billinge.[2] Neutron measurements are generally carried out at spallation sources that have desirable short-wavelength epithermal neutron fluxes. Data collection times vary, depending on the source, sample size and composition, from ~ 20 minutes to 20 hours per data-set. Conventional X-ray measurement protocols use energy resolving solid-state detectors at a high-energy synchrotron where data collection typically takes 8–12 hours per data-set, depending on the sample properties, flux and required Q_{max}. Recently, we have tested a new approach to data collection making use of 2-D image plates as detectors and using very high energy X-rays (~ 100 keV) to compress the scattering data into a relatively narrow angular range.[48] The preliminary result look highly promising, yielding high-quality PDFs from a variety of samples from crystalline nickel to AlF_3 and bismuth vanadium oxide proton-conductor materials. Raw data from the image-plate detector from nickel are shown in Fig. 16, and processed data from AlF_3 in the form of the reduced structure function and PDF are shown in Fig. 17. The quality of the data are apparent from the good signal-noise at high-*Q* in the inset to Fig. 17(a), the relatively small low-*r* fluctuations in *G(r)* coming from systematic errors, and the good fit of the structural model which resulted in structural parameters in agreement with literature values. The nickel data were collected in one second and the lower-*Z* AlF_3 data in 10 seconds. Compared to the typical 8 hours used for the conventional approach this represents an increase in throughput of 3–4 *orders of*

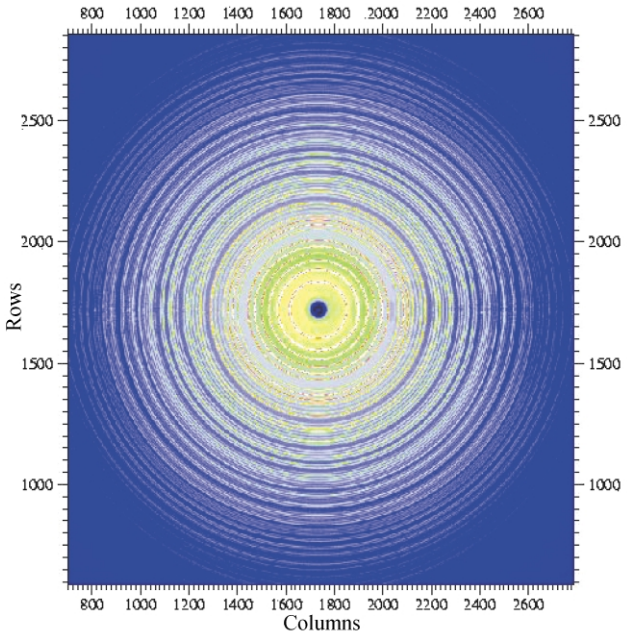

Fig. 16 Raw data from nickel powder collected on a MAR345® image-plate detector. The data were collected at beamline ID1 at the Advanced Photon Source in 1 second of data-collection time.

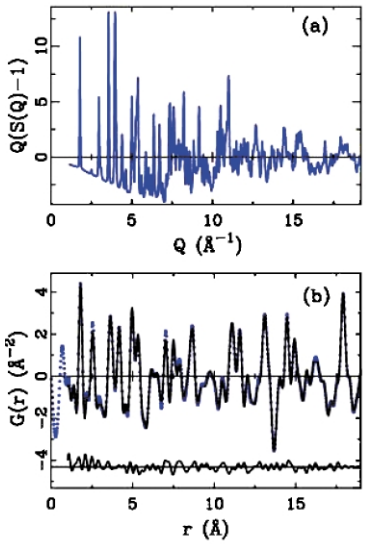

Fig. 17 (a) Reduced structure function and (b) PDF of AlF_3 from data collected using the RA-PDF method. Note the good statistics at high-*Q* and high quality of the PDF despite the short data-collection time. In panel (b) the dots are the data and the solid line is the PDF calculated from the known structure.

magnitude. These measurements are still under development and the data quality and range of applicability are being extended. However, there appears to be tremendous upside potential in using this approach, in part because of the fast data collection time, but also the fact that the measurement is static facilitating measurement of samples in confined geometries and special environments. Future experiments planned that take advantage of these qualities are time-resolved measurements of samples undergoing reaction or under photoexcitation, materials at high-temperatures and under pressure and extensive phase diagram studies.

Conclusions

Here we have presented examples of how total scattering and PDF analysis of X-ray and neutron powder diffraction can be used to solve structural problems that cannot be addressed with traditional crystallographic methods. In this context the PDF analysis technique goes beyond crystallography and captures new structural information. In addition, this type of analysis can be applied in a complementary fashion to conventional crystallography to check the accuracy and validity of the crystallographically determined structure. Given that a crystallographic solution is only an average structure, one cannot be absolutely sure whether the local structure is the same as the average one. If they are not, the average structure is then incorrect and does not capture the critical features that may be responsible for the physical properties of the substance. Thus, ideally, every time a crystal structure is solved crystallographically, a PDF analysis should be done for final validation. We believe the PDF analysis technique promises to be a powerful new weapon in the chemist's arsenal of experimental techniques and will help significantly in our understanding of structures at the atomic level. As the high energy sources become more accessible, the data collection times get very short (using imaging plates, for example) and the software user friendly, the PDF technique has the potential to become nearly a routine type of analysis and a useful tool for structural chemists in the next decades.

Acknowledgements. The authors acknowledge support by DOE through DE-FG02-97ER45651, and NSF through DMR-0304391(NIRT) and CHE-0211029. SJLB acknowledges support from Unita INFM, Italy and the hospitality of Antonio Bianconi and Naurange Saini at U. Roma, "La Sapienza". MGK acknowledges an Alexander von Humboldt Fellowship 2003 and the hospitality of Professor Bernt Krebs at the U. Münster. This work would not have been possible without the tireless efforts of a group of talented individuals, notably Valeri Petkov, Thomas Proffen, Emil Bozin, Xiangyun Qiu and Il-Kyoung Jeong in the Billinge group, and Dr Pantelis Trikalitis, Kasthuri Rangan and Joy Heising in the Kanatzidis group, and our close outside collaborators who appear as coauthors in our papers.

Notes and references

1 B. E. Warren, *X-ray diffraction*, Dover, New York, 1990.
2 T. Egami and S. J. L. Billinge, *Underneath the Bragg-Peaks: Structural Analysis of Complex Materials*, Plenum, Oxford, 2003.
3 T. Egami, in *Local structure from diffraction*, Eds. S. J. L. Billinge and M. F. Thorpe, p. 1 Plenum, New York, 1998.
4 C. N. J. Wagner, *J. Non-Crystal. Solids*, 1978, **31**, 1.
5 Y. Waseda, *The structure of non-crystalline materials*, McGraw-Hill, New York, 1980.
6 I.-K. Jeong, F. Mohiuddin-Jacobs, V. Petkov, S. J. L. Billinge and S. Kycia, *Phys. Rev. B*, 2001, **63**, 205202.
7 A. K. Soper, W. S. Howells and A. C. Hannon, *Rutherford Appleton Laboratory Report*, RAL-89-046, 1989.
8 V. Petkov, *J. Appl. Cryst.*, 1989, **22**, 387.
9 P. F. Peterson, M. Gutmann, Th. Proffen and S. J. L. Billinge, *J. Appl. Crystallogr*, 2000, **33**, 1192.
10 I.-K. Jeong, J. Thompson, A. M. P. Turner and S. J. L. Billinge, *J. Appl. Crystallogr.*, 2001, **34**, 536.
11 Th. Proffen and S. J. L. Billinge, *J. Appl. Crystallogr*, 1999, **32**, 572.
12 (*a*) R. L. McGreevy and L. Pusztai, *Molecular Simulation*, 1988, **1**, 359; (*b*) B. H. Toby, T. Egami, J. D. Jorgensen and M. A. Subramanian, *Phys. Rev. Lett.*, 1990, **64**, 2414.
13 W. Schweika, *Disordered Alloys : Diffuse Scattering and Monte Carlo Simulations*, Springer Verlag, New York, 1998.
14 A. K. Soper, *Chem Phys.*, 1996, **202**, 295.
15 T. R. Welberry, in *From semiconductors to proteins: beyond the average structure*, edited by S. J. L. Billinge and M. F. Thorpe, Kluwer/Plenum, New York, 2002, p. 1.
16 W. Dmowski, B. H. Toby, T. Egami, M. A. Subramanian, J. Gopalakrishnan and A. W. Sleight, *Phys. Rev. Lett.*, 1988, **61**, 2608.
17 S. J. L. Billinge and T. Egami, *Phys. Rev. B.*, 1993, **47**, 14386.
18 S. J. L. Billinge, R. G. DiFrancesco, G. H. Kwei, J. J. Neumeier and J. D. Thompson, *Phys. Rev. Lett.*, 1996, **77**, 715.
19 D. Louca, T. Egami, E. L. Brosha, H. Roder and A. R. Bishop, *Phys. Rev. B.*, 1997, **56**, R8475.
20 E. S. Bozin, S. J. L. Billinge, G. H. Kwei and H. Takagi, *Phys. Rev. B*, 1999, **59**, 4445.
21 V. Petkov, I-K. Jeong, J. S. Chung, M. F. Thorpe, S. Kycia and S. J. L. Billinge, *Phys. Rev. Lett.*, 1999, **83**, 4089.

22 V. Petkov, I-K. Jeong, F. Mohiuddin-Jacobs, Th. Proffen and S. J. L. Billinge, *J. Appl. Phys.*, 2000, **88**, 665.
23 J. C. Mikkelson and J. B. Boyce, *Phys. Rev. Lett.*, 1982, **49**, 1412.
24 V. Petkov, S. J. L. Billinge, S. D. Shastri and B. Himmel, *Phys. Rev. Lett.*, 2000, **85**, 3436.
25 R. L. Whetten, J. T. Khoury, M. M. Alvarez, S. Murthy, I. Vezmar, Z. L. Wang, P. W. Stephens, C. L. Cleveland, W. D. Luedtke and U. Landman, *Adv. Mater.*, 1996, **8** , 426.
26 A. P. Alivisatos, *J. Phys. Chem.*, 1996, **100**, 13226.
27 V. Petkov, S. J. L. Billinge, J. Heising and M. G. Kanatzidis, *J. Am. Chem. Soc.*, 2000, **122**, 11572.
28 V. Petkov, S. J. L. Billinge, P. Larson, S. D. Mahanti, T. Vogt, K. K. Rangan and M. G. Kanatzidis, *Phys. Rev. B.*, 2002, **65**, 92105.
29 V. Petkov, P. N. Trikalitis, E. S. Bozin, S. J. L. Billinge, T. Vogt and M. G. Kanatzidis, *J. Am. Chem. Soc.*, 2002, **121**, 10157.
30 M. G. Kanatzidis, R. Bissesssur and D. C. DeGroot, *Chem. Mater.*, 1993, **5**, 595.
31 W. M. R. Divigalpitiya, R. F. Frindt and S. R. Morrison, *Science*, 1989, **246**, 369.
32 S. J. Hibble, I. D. Fawcett and A. C. Hannon, *Inorg. Chem.*, 1997, **36**, 1749.
33 (*a*) S. J. Hibble and I. D. Fawcett, *Inorg. Chem.*, 1995, **34**, 500; (*b*) S. J. Hibble, I. D. Fawcett and A. C. Hannon, *Acta Crystallogr.*, 1997, **53**, 604.
34 (*a*) S. J. Hibble, S. P. Cooper, A. C. Hannon, S. Patat and W. H. McCarroll, *Inorg. Chem.*, 1998, **37**, 6839; (*b*) S. J. Hibble, S. P. Cooper, S. Patat and A. C. Hannon, *Acta Crystallogr. B*, 1999, **55**, 683.
35 S. J. Hibble and A. C. Hannon, in *From semiconductors to proteins: beyond the average structure* edited by S. J. L. Billinge, and M. F. Thorpe, Kluwer/Plenum, New York, 2002, p. 129.
36 L. E. Aleandri and R. E. McCarley, *Inorg. Chem.*, 1988, **27**, 1041.
37 A. C. W. P James and J. B. Goodenough, *J. Solid State Chem.*, 1988, **76**, 87.
38 (*a*) J. Livage, *Chem. Mater.*, 1991, **3**, 578; (*b*) J. Livage, O. Pelletier and P. Davidson, *J. Sol-Gel Sci. Techn.*, 2000, **19**, 275.
39 L. E. Brus, *J. Phys. Chem.*, 1986, **90**, 2555.
40 D.-L. Price and M-L. Saboungi, in *Local structure from diffraction*, Eds. S. J. L. Billinge and M. F. Thorpe, Plenum, New York, 1998, p. 23.
41 P. Armand, M-L. Saboungi, D. L. Price, L. Iton, C. Cramer and M. Grimsditch, *Phys. Rev. Lett.*, 1997, **79**, 2061.
42 J. Eckert, C. M. Draznieks and A. K. Cheetham, *J. Am. Chem. Soc.*, 2002, **124**, 170.
43 V. Petkov, S. J. L. Billinge, T. Vogt, A. S. Ichimura and J. L. Dye, *Phys. Rev. Lett.*, **89**, 75502.
44 (*a*) J. L. Dye, *Inorg. Chem.*, 1997, **36**, 3816; (*b*) G. Allan, M. G. DeBacker, M. Lannoo and J. Lefebre, *Europhys. Lett.*, 1990, **11**, 49; (*c*) D. J. Singh, H. Krakauer, C. Haas and W. E. Pickett, *Nature*, 1993, **365**, 39; (*d*) T. A. Kaplan, R. Rencsok and J. F. Harrison, *Phys. Rev. B*, 1994, **50**, 8054.
45 S.-J. Hwang, V. Petkov, K. K. Rangan, S. Shastri and M. G. Kanatzidis, *J. Phys. Chem. B.*, 2002, **106**(48), 12453–12458.
46 R. Patschke, J. D. Breshears, P. Brazis, C. R. Kannewurf, S. J. L. Billinge and M. G. Kanatzidis, *J. Am. Chem. Soc.*, 2001, **123**, 4755.
47 K.-Y. Choi, R. Patschke, S. J. L. Billinge, M. J. Waner, M. Dantus and M. G. Kanatzidis, *J. Am. Chem. Soc.*, 1998, **120**, 10706.
48 P. J. Chupas, X. Qiu, C. P. Grey and S. J. L. Billinge, *J. Appl. Crystallogr.*, 2003, **36**, 1342.